

# The influence of tempering and annealing on the microstructure and sliding wear response of G350 grey cast iron

Ronnie G. Woodward<sup>a,\*</sup>, Athanasios Toumpis<sup>b</sup>, Alexander Galloway<sup>b</sup>

<sup>a</sup> Advanced Materials Research Laboratory, Department of Mechanical & Aerospace Engineering, University of Strathclyde, Glasgow, UK

<sup>b</sup> Department of Mechanical & Aerospace Engineering, University of Strathclyde, Glasgow, UK

## ARTICLE INFO

### Keywords:

Sliding wear  
Oxidative wear  
Cast iron  
Tempering

## ABSTRACT

The present study investigates the tribological properties of G350 grey cast iron in various microstructural conditions. Quench and temper heat treatments were conducted at four tempering temperatures, from 400 °C to 700 °C, to produce a range of tempered martensitic disc samples. Pins were slow furnace-cool annealed to produce a coarse pearlitic microstructure with some areas of ferrite. These samples were then used in pin-on-disc sliding wear tests. Hardness decreased with tempering temperature, from 400HV at 400 °C to 200HV at 700 °C. The two spheroidized carbide discs produced higher volume losses than the two acicular martensitic discs due to instability of the oxide layer on the softer substrate. Subsurface deformation was visible in the annealed pins and spheroidized discs which consisted of deformed cementite lamellae in the direction sliding and strained ferrite grains.

## 1. Introduction

Grey cast iron is a versatile ferrous alloy used in a wide variety of industrial applications [1]. High molten fluidity and low thermal shrinkage allow cast irons to be used for components with complex geometries [2] such as crankshafts and engine cylinder blocks. However, certain applications of cast iron require a combination of hardness, toughness, and wear resistance. This is particularly the case for automotive or pumping components such as selector forks, cam lobes, or slipper pads, where the material is sliding under load. In these instances the mechanical integrity of the material is imperative to prevent serious failure, and therefore tempered martensitic matrices are optimal due to their balance of mechanical properties. Industrial cast irons typically have a high alloying content, allowing for a multitude of possible microstructures and making them readily heat treatable [3]. Tempered martensitic matrices are therefore easily producible for grey cast irons [4].

Research on the sliding wear effects of tempering focusses primarily on steels. Ouyang et al. [5] investigated the sliding wear and mechanical properties of tempered 4Cr13 steel at various loads and sliding speeds. The researchers found that mass loss increased with increasing tempering temperature and noted a transition to severe wear for all tested combinations at higher loads and sliding speeds. Wei et al. [6]

studied the effects of tempering on the high temperature wear rate of H13 die steel. The authors found that wear resistance was not proportional to the hardness of the tempered samples, and that in some instances, the softer sample had a lower wear rate due to the having higher fracture toughness. This was postulated to be due to temper embrittlement in the harder samples caused by the precipitation of carbides on the grain boundaries. Trevisiol et al. [7] investigated the effect of varying tempering temperature on the sliding wear properties of 35NCD16 steel. The authors noted that hardness decreased from 600HV to 350HV when tempering temperature increased from 200 °C to 400 °C. At approximately 430HV, from tempering at 400 °C, the microstructure changed significantly from martensitic laths to equiaxed grains with carbides.

Research articles on the quench and tempering effects of cast iron in sliding wear are few and focus on comparisons between martensitic versus austempered microstructures, or compare the effect of alloying content on the tempering response. Haseeb et al. [8] compared the performance of austempered versus quench and tempered ductile iron. Oxidation was found to be the dominant wear mechanism occurring for both conditions, and the austempered samples were found to be slightly more wear resistant than tempered martensite. However, the researchers did not perform an examination of the subsurface deformation in detail and did not show how the worn surfaces change with increasing

\* Corresponding author.

E-mail address: [ronnie.woodward@strath.ac.uk](mailto:ronnie.woodward@strath.ac.uk) (R.G. Woodward).

<https://doi.org/10.1016/j.wear.2022.204283>

Received 29 September 2021; Received in revised form 20 January 2022; Accepted 9 February 2022

Available online 11 February 2022

0043-1648/© 2022 The Authors. Published by Elsevier B.V. This is an open access article under the CC BY license (<http://creativecommons.org/licenses/by/4.0/>).

applied load. Such factors are important in evaluating the tribological response of the alloy.

Vadiraj et al. [9] studied the sliding wear properties of various cast irons at various tempers. The researchers found that higher alloyed cast irons were less softened by the tempering treatment, and that tempering at 400 °C provided an optimum balance of wear resistance, hardness, and toughness. However, the researchers only show and discuss the quantitative data produced from the heat treatments and sliding wear tests, instead of also including qualitative data such as characterisation of subsurface deformation and inspection of the worn surfaces. Moreover, only one set of sliding parameters was used, instead of altering key variables such as speed or load. This serves to compare the numerous alloys tested but does not show if the wear response changes over different conditions.

Little research exists on the effects of high temperature tempering for grey cast irons in sliding while altering the applied load, inspecting the worn surfaces, and characterising the subsurface deformation. The present study rectifies this through subjecting industrial grey cast iron to four degrees of high temperature tempering. The various heat treated samples are then subjected to pin-on-disc testing using three loads to characterise the sliding wear response of the material with load. Additional inspection of the worn surfaces and subsurface deformation then takes place, along with the scientific discussion of the results and significance of the findings.

## 2. Materials & methods

### 2.1. Materials

Both the pin and the disc (Section 2.2.) were made of G350 cast iron (Table 1), in different microstructural conditions.

Cast iron was received in the martensitic condition with type I-A/C-5 graphite flakes in accordance with ISO 945 [10]. Pin samples were furnace-cool annealed from 900 °C to room temperature over 12 h. Discs were oil quenched from 900 °C, followed by tempering at four temperatures, hereafter referred to as 700C (tempered at 700 °C), 600C, 500C, and 400C. Tempering duration was 24 hours for all discs. Table 2 shows a summary of both heat treatments.

Cast iron was examined in various microstructural combinations to (a) enhance the scientific tribological novelty of the current study, and (b) to provide industrial relevance by employing microstructural conditions seen for many cast irons in engineering applications. Pearlitic cast irons see everyday usage in the automotive industry as brake discs in numerous vehicles. Martensitic cast irons feature in the aforementioned long term applications such as slipper pads in hydraulic rotary piston pumps.

The detrimental effects of using self-mated materials in sliding are avoided through the different heat treatments producing markedly different microstructural conditions of the cast iron pins and discs. These effects, such as the high likelihood of self-mated austenitic stainless steels to gall [11,12], can result in seizure and high wear rates. However, as the pins exhibit a coarse pearlitic and ferritic matrix, and the discs exhibit tempered martensitic matrices, the similarity is reduced which avoids this problem. These different microstructural conditions effectively mean that the samples are not self-mated, and can instead be treated as different materials despite having the same chemical composition.

**Table 1**  
Nominal elemental composition of G350 cast iron (wt%).

Material	C	Cr	Cu	Mn	Mo	P	S	Si	Fe
G350	3.35	0.25	0.65	0.70	0.25	0.150	0.055	2.75	Bal.

**Table 2**  
Summary of sample heat treatments.

Sample	Heat Treatment	Type	Temperature (°C)	Duration (Hours)	Resultant Microstructure
Pins	Anneal	Furnace-cool	900 to room temperature	12	Coarse pearlite + ferrite
Discs	Quench & Temper	Oil	400, 500, 600, 700	24	Tempered martensite

### 2.2. Methods

Wear behaviour was examined using dry pin-on-disc sliding wear tests (Table 3), and followed the procedure of ASTM G99 [13]. The pin-on-disc testing configuration was chosen to allow for comparisons to the reviewed literature which used the same configuration, and to simulate the sliding conditions seen in the most relevant industrial examples of brake discs and slipper pads. Each test was replicated three times for repeatability, and the standard deviation calculated. All tests were conducted in ambient laboratory conditions. Sample mass losses were measured using an analytical balance accurate to 0.0001g. The values of mass loss were then converted into volume losses by dividing through by density using a value of 0.0073 g/mm<sup>3</sup>.

Microstructures were characterised using an inverted microscope. Wear scars were examined using scanning electron microscopy (SEM) for damage assessment, and stylus profilometry to visualise their 2D cross-sections. X-ray diffractometry (XRD) was used to identify microstructural phases of the discs. Disc wear scar roughness was measured perpendicularly to the direction of sliding using a 2D contact profilometer from three measurements from each repeated test (resulting in nine measurements for each sliding combination), and the mean value and standard deviation calculated. Micro indentation hardness was measured with 500gf and a dwell time of 15 s, with values averaged from 10 measurements and the standard deviation calculated. Macro indentation hardness was measured with 5kgf and a dwell time of 15 s, with values averaged from 10 measurements and the standard deviation calculated.

## 3. Results

Furnace-cool annealing caused the as-received martensitic matrix of the G350 pins to transform into coarse pearlite and ferrite (Fig. 1). Graphite morphology remained unchanged.

The quench and tempering process of the discs produced four distinct martensitic microstructures corresponding to each tempering temperature (Fig. 2). The 400C and 500C discs displayed acicular martensitic microstructures interspersed by the unchanged graphite flakes. An evolution can be observed between 400C and 500C where a rounding of the martensite needles occurred due to the increasing temperature (Fig. 2(b)).

The 600C and 700C discs appeared overly tempered and spheroidized [14], with small carbide globules present throughout the matrix. A coarsening of the carbide globules can be seen between 600C and 700C where the increased temperature allowed the carbides to further spheroidize [15] (Fig. 3).

X-ray diffractometry (XRD) phase identification showed that the dominant phase of all four disc microstructures was alpha ferrite (Fig. 4). The 400C discs showed the same ferrite peaks but with lower intensity, due to additional presence of BCT martensite. This is

**Table 3**  
Summary of pin-on-disc methodology.

Pin Material	Disc Material	Pin dia (mm)	Disc dia (mm)	Load (kg)	Sliding Speed (m/s)	Distance (m)	Pin and Disc Surface Roughness, Ra ( $\mu\text{m}$ )
G350	G350	6	70	2, 4, 6	0.50	2538	0.3 $\pm$ 0.1

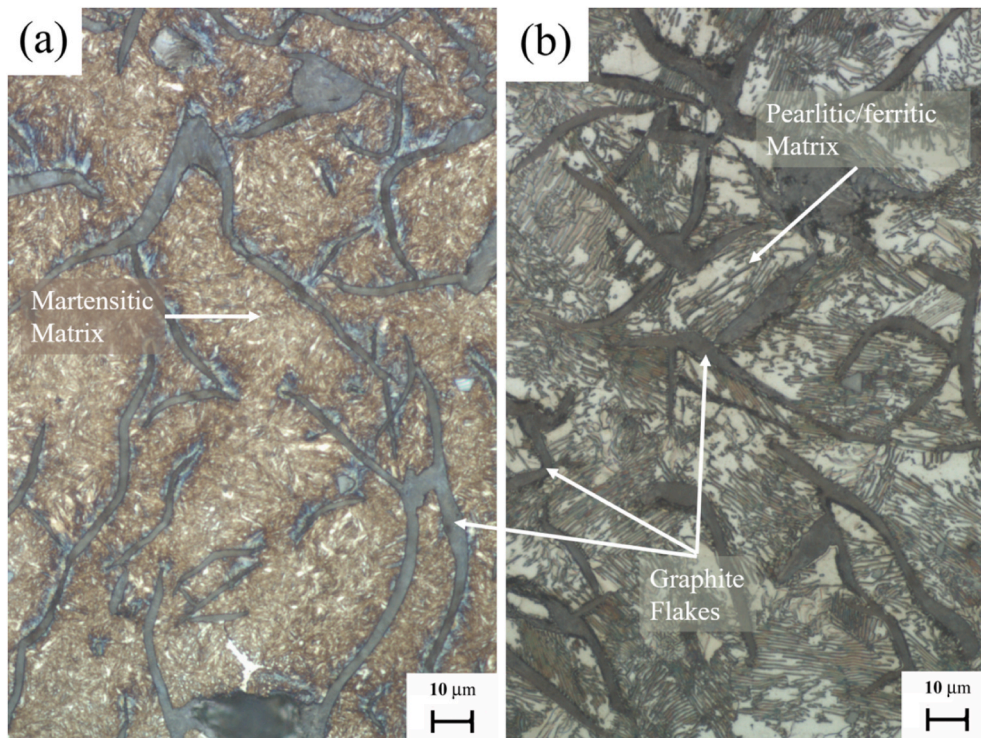


**Fig. 1.** Microstructures of (a) as-received cast iron and (b) furnace-cool annealed pins (b). [x500 – nital].

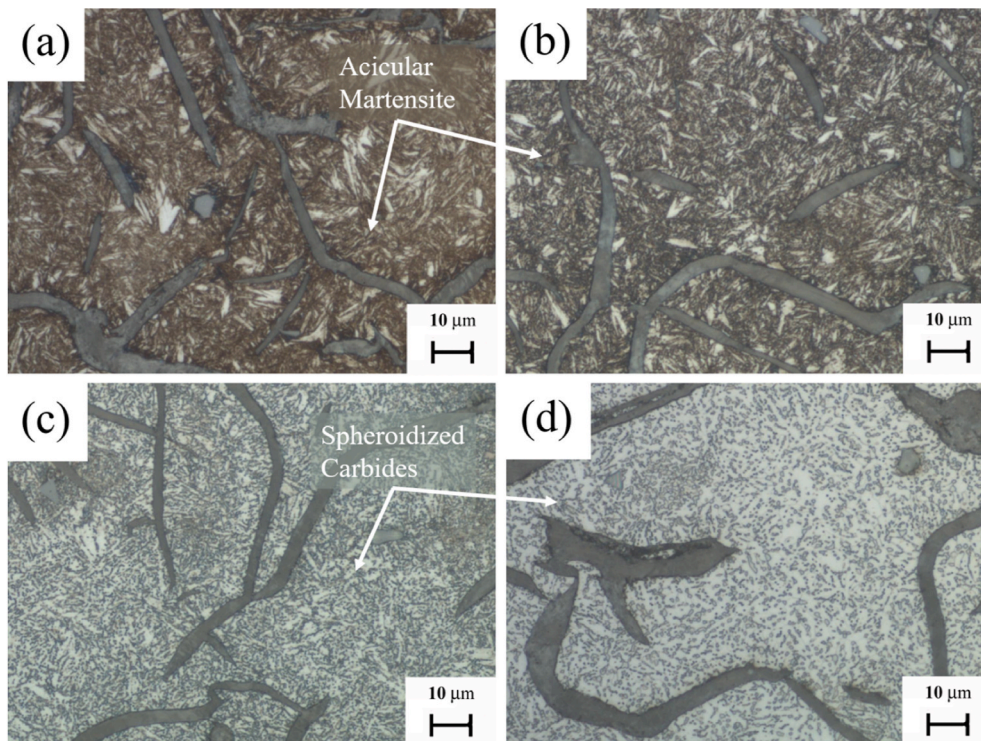


**Fig. 2.** Microstructure of the discs tempered at (a) 400 °C (b) 500 °C (c) 600 °C (d) 700 °C. [x500 – nital].

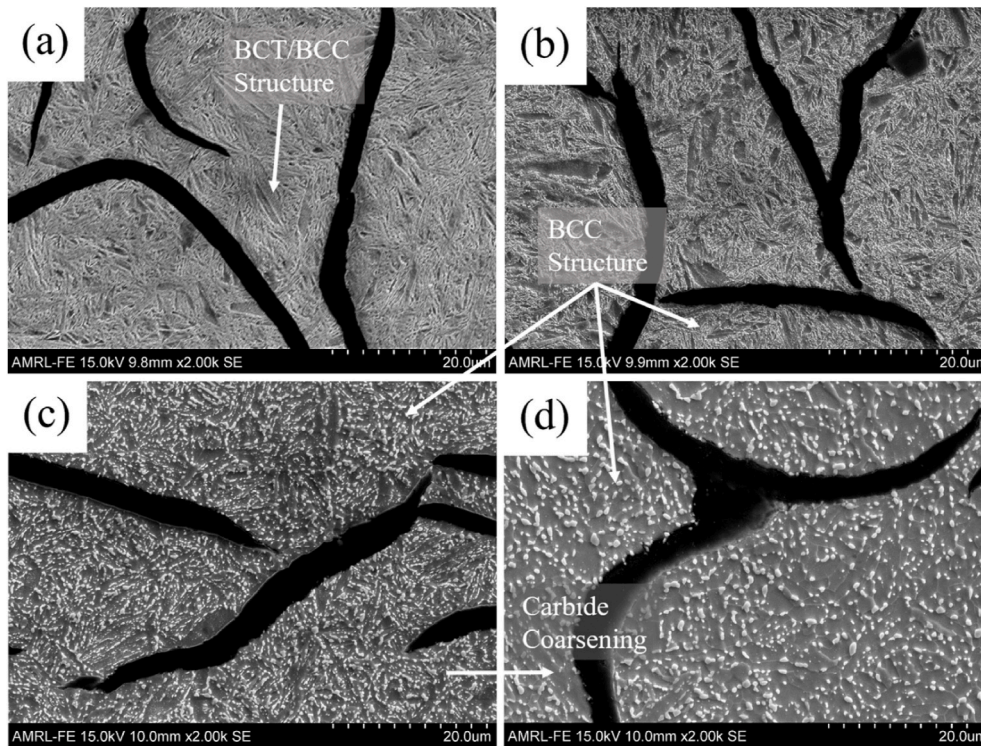


Fig. 3. Microstructure of the discs tempered at (a) 400 °C (b) 500 °C (c) 600 °C (d) 700 °C. [x2000 – nital].

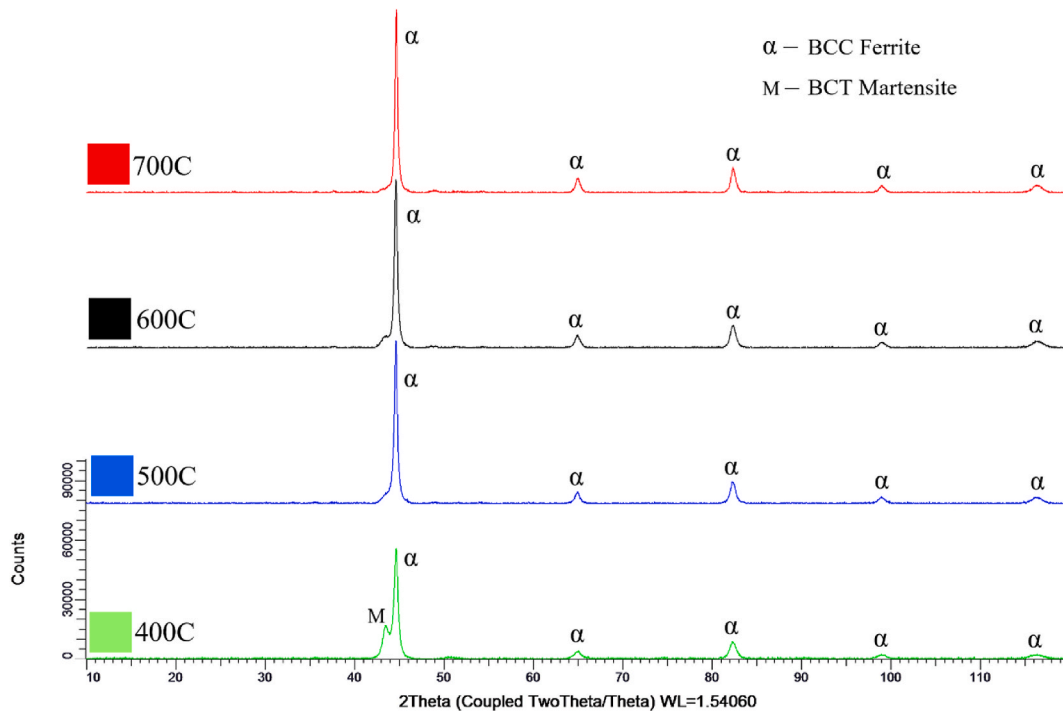


Fig. 4. XRD compositional peaks of the four disc conditions.

evidenced by a peak identified as such for the 400C disc.

Micro and macro indentation hardness measurements (Fig. 5) showed that hardness values decreased with increasing tempering temperature from 400HV at 400C to 200HV at 700C. The annealed pins were also approximately 200HV. The graph also displays error bars which show the magnitude of standard deviation of the ten measurements taken to produce each hardness value.

The pin on disc results show the volume loss values of the discs (Fig. 6) and respective pins (Fig. 7) from sliding wear. The graphs also display error bars for each trend line which show the magnitude of standard deviation of the three repeats conducted to produce each volume loss value.

For both discs and pins, the standard deviation of results generally increased with load. The disc volume loss values (Fig. 6) show that the

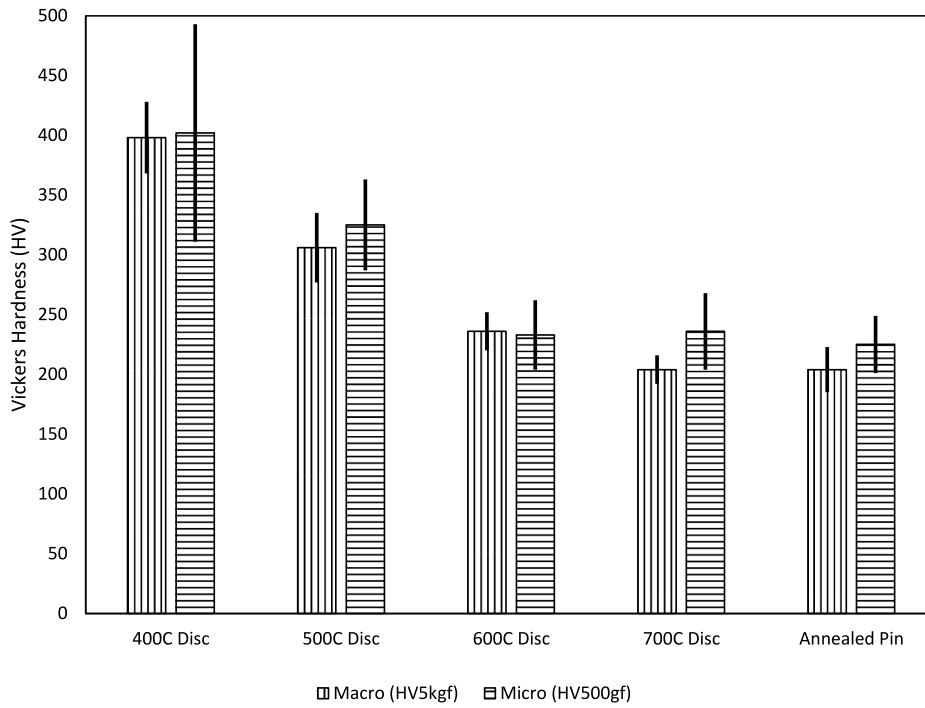


Fig. 5. Micro and macro indentation Vickers hardness values.

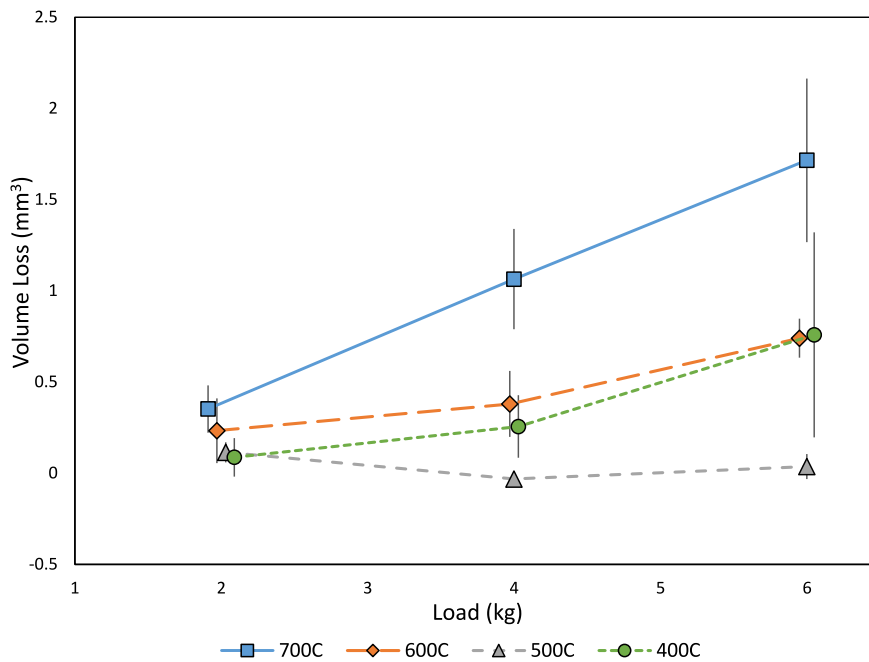


Fig. 6. Disc volume loss results.

700C discs experienced the highest volume losses for all loads, and that the 500C discs experienced the lowest volume losses for all loads, with the 400C and 600C discs falling in between these extremes.

The pin volume losses (Fig. 7) generally increased and diverged with load.

Examining the worn surfaces using SEM showed damage mechanisms occurring near the end of the test (such examinations do not reveal wear mechanisms occurring at the start of the test as evidence would have been erased from further sliding cycles). Oxidative wear was

common for all discs and was the dominant mechanism at lighter loads (Fig. 8). Many worn surfaces were covered in oxide islands with little damage to the metallic surface. Residual grinding lines were often observed indicating that the pin did not wear itself into the disc surface.

At higher loads, further damage of the metallic matrix took place which was seen through the presence of scuffing, scoring, and ploughing. The softer discs deformed more plastically than the harder discs.

The difference between mild oxidative wear and severe mechanical wear was also observed in the cross-sectional profiles of the disc wear

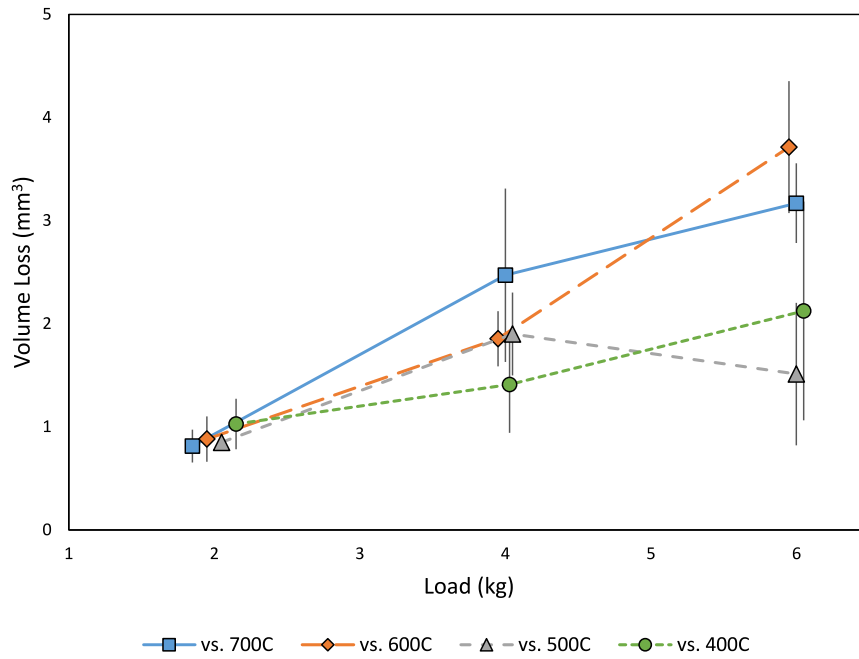


Fig. 7. Pin volume loss results.

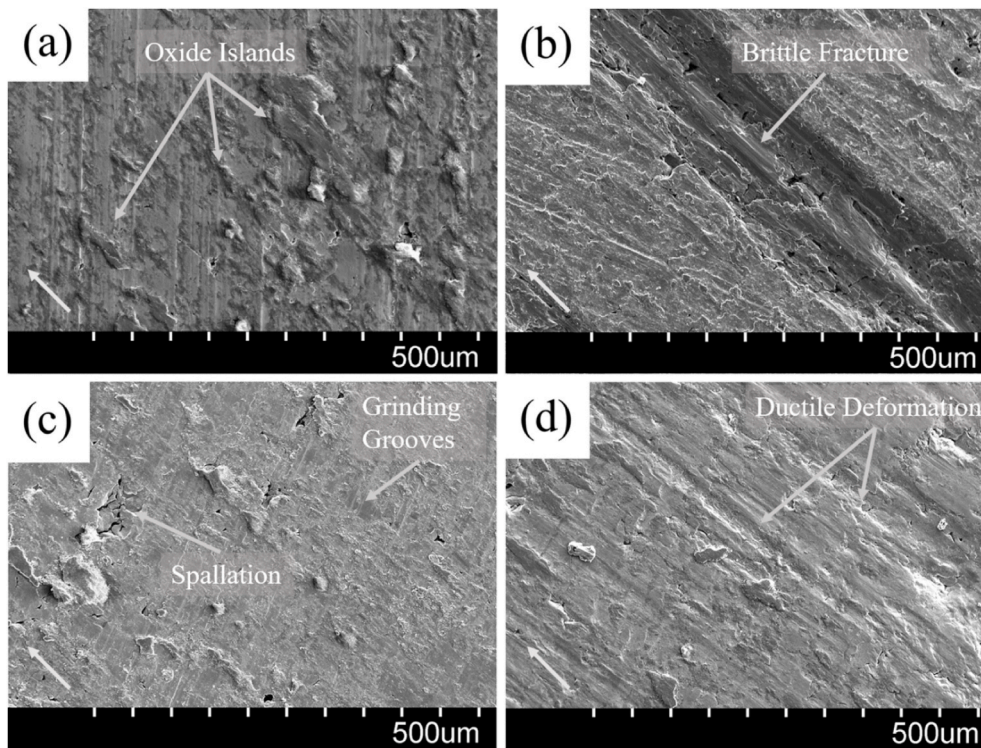


Fig. 8. Resultant disc damage on (a) 400C 2 kg, (b) 400C 6 kg, (c) 700C 2 kg, (d) 700C 6 kg [x100].

scars (Fig. 9). The mild wear scars were indistinguishable from the unworn surface cross-section (seen from 0 to 2 mm and from 8 to 10 mm). Conversely, the more worn wear scars showed peaks and troughs of mechanical damage mechanisms.

Disc wear scar surface roughness (Fig. 10) showed that at 2 kg and 4 kg, roughness increased with tempering temperature. As load increased to 4 kg, 700C and 600C increased in roughness while 500C and 400C decreased in roughness. Moreover, the order of roughness was

maintained. At the highest load, three of the four combinations showed large standard deviations. 700C, 600C, and 500C displayed a decrease in roughness, relative to 4 kg applied load, and were in the same order. Conversely, the 400C scars instead increased in surface roughness and display a large standard deviation.

Oxide coverage varied with load. At 2 kg, the oxide often appeared as smaller, crumbly islands on the surface, frequently worn off as powder. At higher loads, the oxide was an adhered layer which would instead

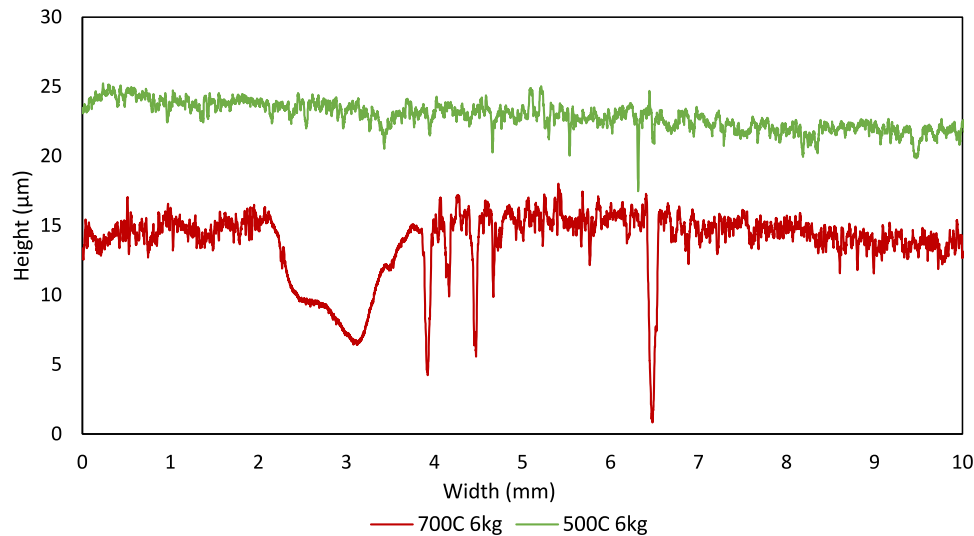


Fig. 9. Cross-sectional profiles of (green) oxidative wear scar and (b) oxidational + mechanical damage wear scar. (For interpretation of the references to colour in this figure legend, the reader is referred to the Web version of this article.)

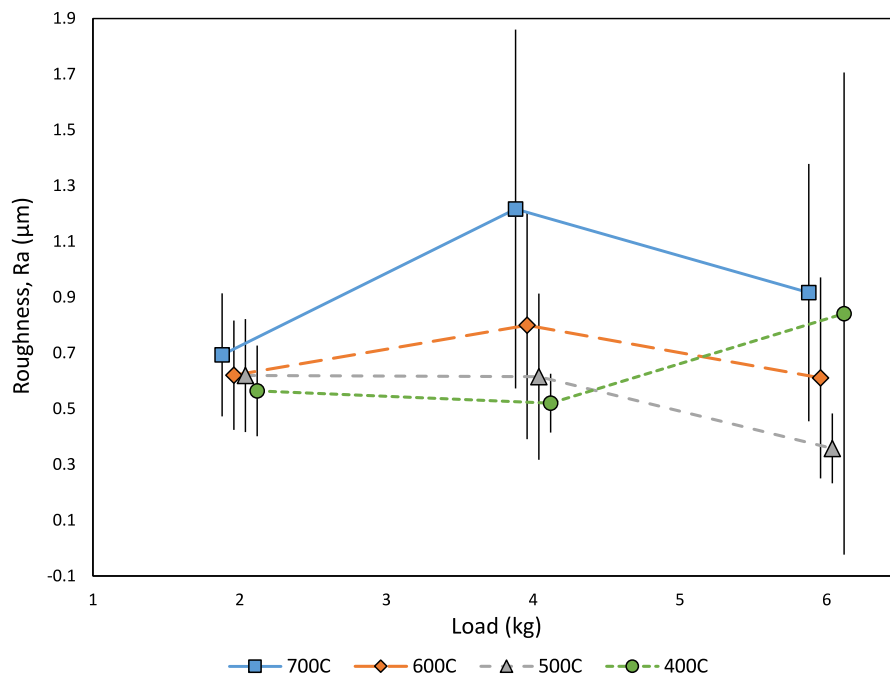


Fig. 10. Wear scar surface roughness, Ra.

spall, exposing fresh metal underneath to then oxidise (Fig. 11).

Fewer oxide products were observed on the worn surfaces of the annealed pins, either due to a lack of oxidation occurring or because of transfer to the disc counter body. Many pins instead displayed highly polished areas with smooth, featureless surfaces at 2 kg applied load (Fig. 12). Such polishing effects have previously been observed for the same alloy [16]. In these particular areas, the only notable features were the exposed graphite cavities (Fig. 13) from spallation.

At 6 kg applied load, more damage mechanisms occurred on the pin worn surfaces (Fig. 14) such as increased oxidation and brittle ploughing. The pins worn against the acicular martensitic discs and the pins worn against the spheroidized carbide discs wore differently, whereby the former experienced more brittle ploughing with the latter

experiencing more oxidation.

Microstructural subsurface deformation was readily visible in the annealed pin cross-sections (Fig. 15). Cementite lamellae deformed in the direction of sliding, parallel to the worn surface. Other features of subsurface deformation include ferrite grain strain and fracture of lamellae (Fig. 16).

Dark areas surrounded the lamellae fracture sites (Fig. 17), highlighting the voids left from delamination between the ferrite matrix and cementite plate.

Near to the surface, lamellae sometimes refined and compacted into a mechanically mixed carbide-oxide layer (Fig. 17, Table 4).

Subsurface deformation was also visible in the spheroidized carbide globule discs (Fig. 18). These discs only displayed such deformation

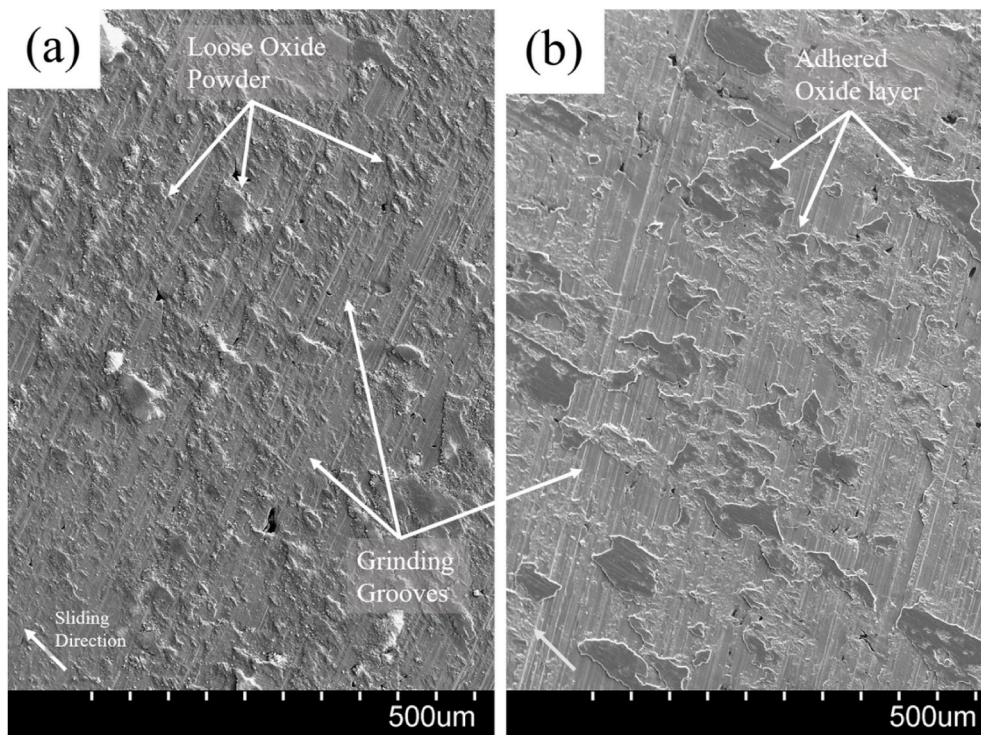


Fig. 11. Resultant disc damage on 500C discs from loads of (a) 2 kg, (b) 6 kg [x100].

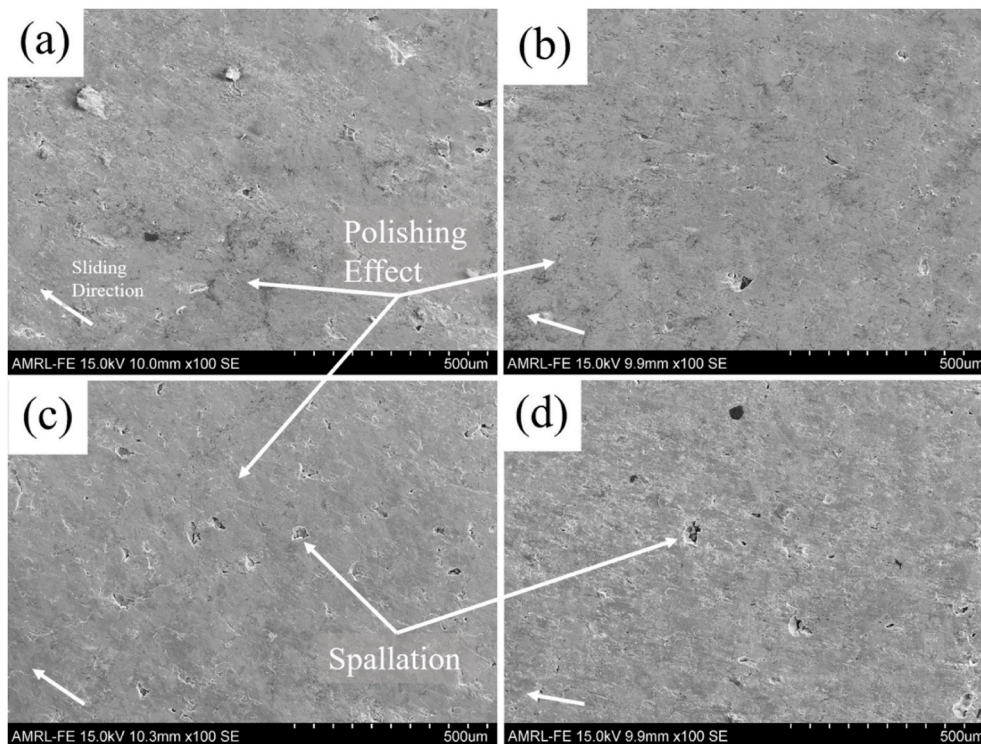


Fig. 12. Resultant 2 kg pin damage on (a) 400C (b) 500C (c) 600C (d) 700C pins. [x100].

through strained and directional ferrite grains. The strained directional ferrite is readily discernible in comparison to the bulk microstructure of the disc sample, showing non-directional equiaxed grains of ferrite.

#### 4. Discussion

##### 4.1. Carbide morphology

Hardness values are good indicators of wear resistance, however, microstructural morphology is also critical in governing the wear

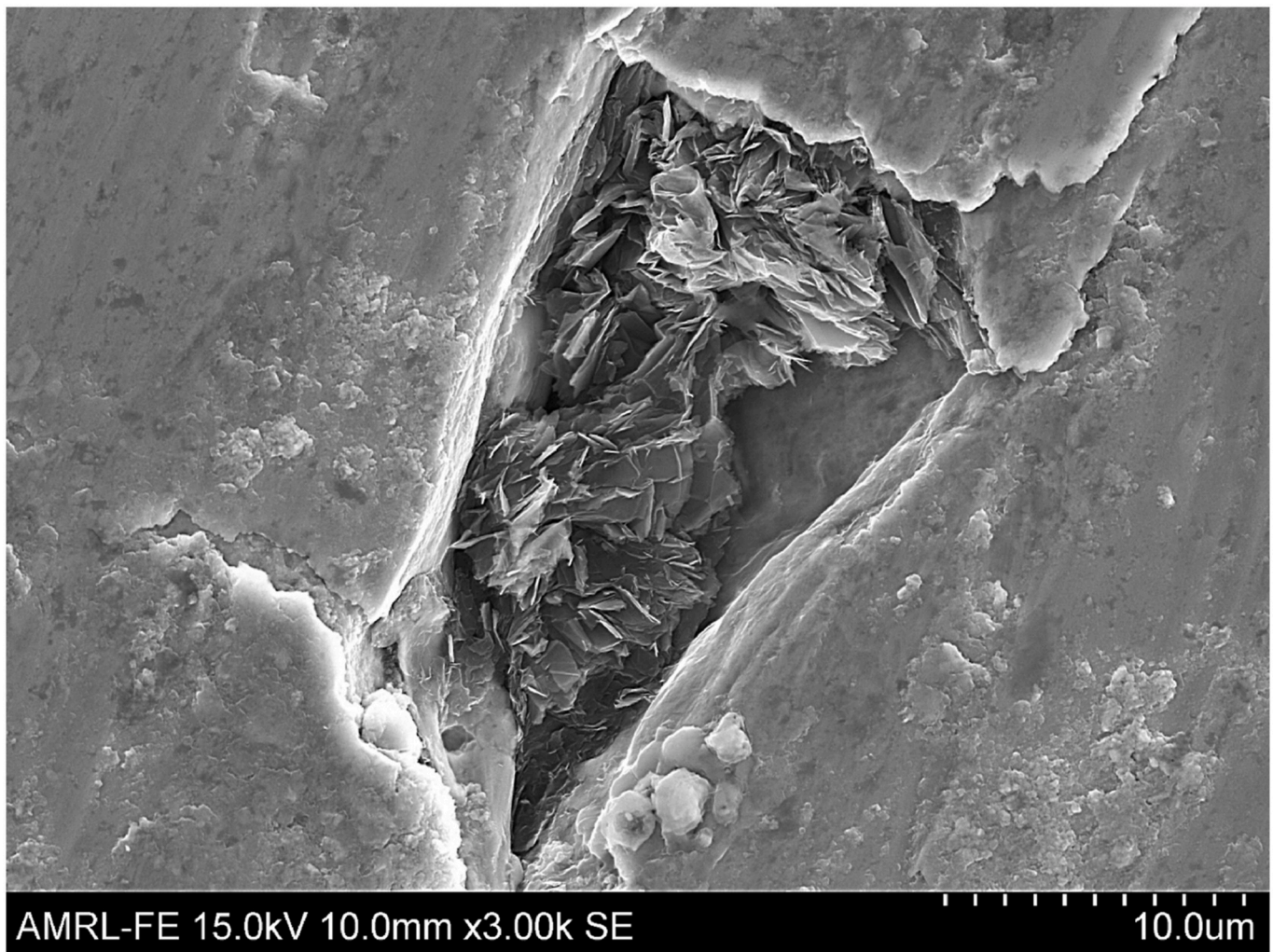


Fig. 13. Exposed graphite flake following spallation of the metallic cavity roof. [x2000].

response. This has been documented by Diao et al. [17], Zambrano et al. [18], and Haseeb et al. [8] who tested steels and cast irons with the same hardness but different microstructures. In the present study, the 600C discs, 700C discs, and annealed pins have similar hardness values (Fig. 5). However, different wear responses arise from the increased coarsening of the carbide globules from 600C to 700C, and the pearlitic/ferritic microstructure of the annealed pins. Mechanistically, such differences between 600C and 700C may arise from the coarsening of carbide globules resulting in more abrasive action between the two worn surfaces [19], causing self-damage or wear to the counter body. Moreover, the coarsening of the globules reduces their reinforcement effect on the ferrite matrix, producing a greater vulnerability to damage mechanisms such as scoring and ploughing. Regarding the annealed pins, the mix of coarse pearlite and ferrite (Fig. 1) bestows a harder bulk microstructure due to having cementite lamellae – plate morphology – instead of free carbide globules, resulting in greater resistance to deformation.

#### 4.2. Crystallographic transformations

Disc hardness decreases with tempering temperature (Fig. 5), which has also been observed by Vadiraj et al. [9]. The 400C discs show the maximum hardness (400HV), followed by the 500C discs (300HV). This decrease is due to two factors: the transformation from BCT martensite to BCC ferrite at approximately 400 °C, and the loss of acicular morphology between 500 °C and 600 °C. The former transformation is

observed through the XRD compositional analyses for the 400C discs (Fig. 4), and indicates that the process of ferrite transformation is partially underway but not complete at 400 °C. In contrast, the 500C disc scan only displays peaks for BCC ferrite indicating complete transformation. Despite this transformation, the 500C discs still display an acicular microstructure (Figs. 2 and 3), where the original acicular morphology of the BCT martensite remains while the underlying matrix has transformed to BCC ferrite. This change from acicular martensite to carbide globules within equiaxed grains of ferrite has also been observed by Trevisiol et al. [7], who noted this occurred around 500 °C for their 35NCD16 steel. In the present study, optical observation showed little difference between 400C and 500C discs, apart from a slight rounding of the needles (Fig. 2). Through SEM, more contrast is seen (Fig. 3) where coarsening and rounding of the needles indicate the eventual change to spheroidized carbides. The decrease in hardness from 500C to 600C (Fig. 5) indicates that the change to ferrite with carbide globules also influences mechanical properties.

#### 4.3. Oxidative wear

Despite the different hardness levels of the discs, their volume loss values (Fig. 6) are similar. This is due to the dominance of oxidative wear [20–22] for most sliding pairs. Such typical wear behaviour is often seen for cast iron and alloy steels, and has been observed by Haseeb et al. [8] for cast irons in sliding. In the absence of wear transitions [23], oxidative wear produces little variation, even with

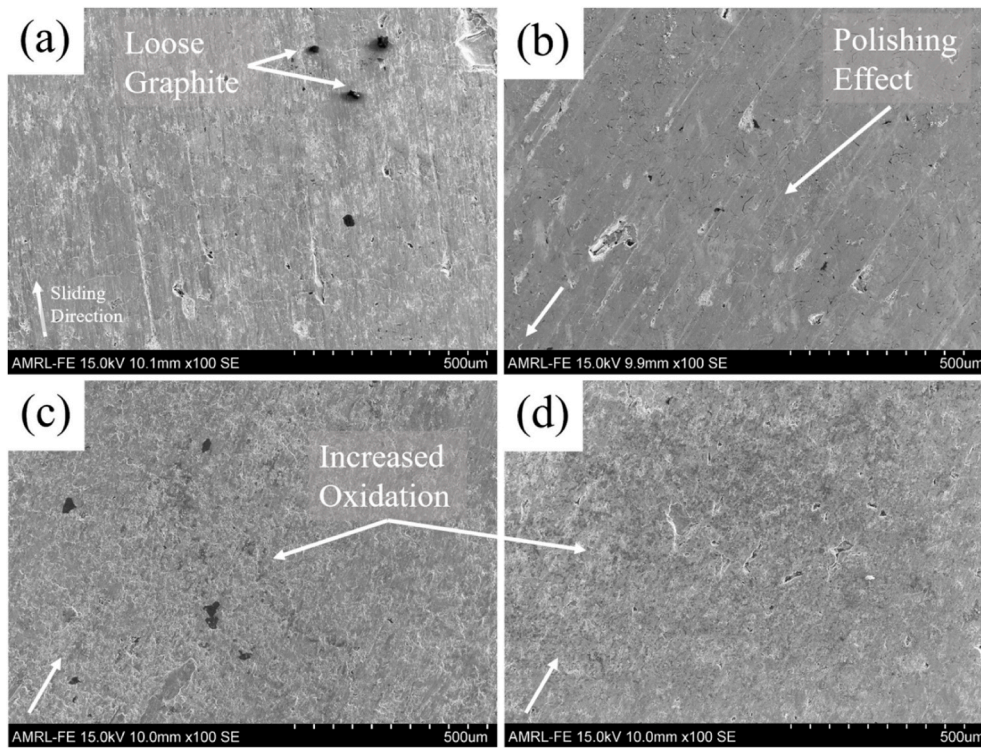


Fig. 14. Resultant 6 kg pin damage on (a) 400C (b) 500C (c) 600C (d) 700C pins. [x100].

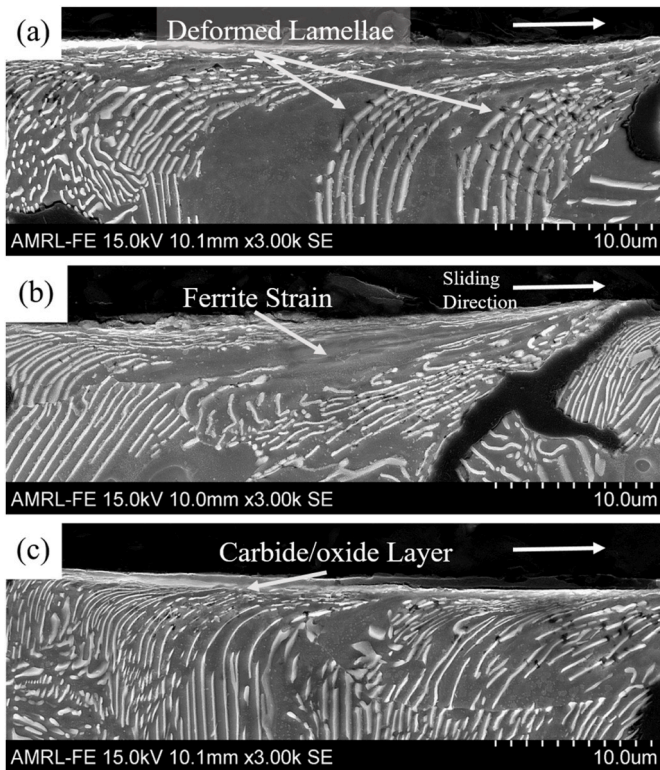


Fig. 15. Microstructural subsurface deformation of annealed pins. [x3000 – nital].

changing parameters. Tribology researchers often categorize wear into a binary choice of mild or severe to simplify analysis [20,24,25]. Mild wear results in low volume losses and oxidation which does not mechanically damage the underlying matrix. Severe wear produces

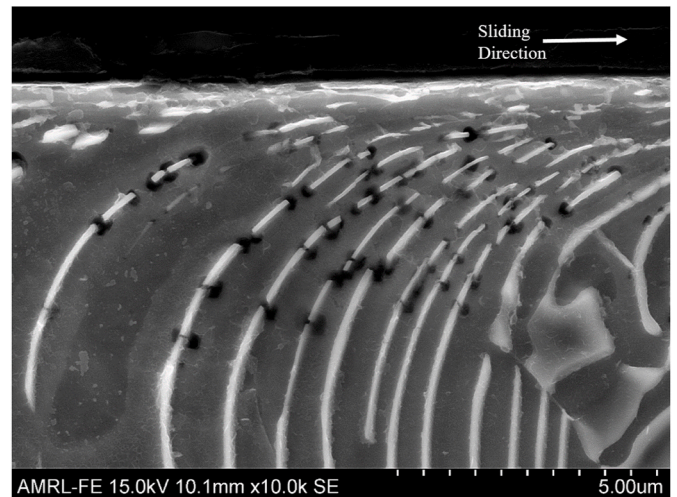


Fig. 16. Fractured cementite lamellae from sliding deformation. [x10000 – nital].

mechanical, metallic damage of the matrix resulting in scoring, ploughing, smearing, and spallation. Mild and severe wear can be distinguished through visual inspection of the wear scar, with mild wear appearing a discoloured red/brown due to oxidation, and severe wear displaying a bright, reflective metallic colour due to the exposed damage metallic matrix.

In the present study, mild wear occurs after establishment of an oxide glaze layer [26–29], and this persists, in most cases, for all loads in the present study. Furthermore, inspection of the disc wear scars (Figs. 8 and 11) shows predominantly oxide islands, with other forms of damage only occurring at the highest applied load. The cross-sectional profiles (Fig. 9) show that the oxidative mild cross-section worn area is barely distinguishable from the unworn surface, whereas the severe cross-section worn area has large peaks and troughs from ploughing



Fig. 17. Carbide/oxide surface layer and EDS points on 500C 6 kg disc. [x10000 – nital].

Table 4

EDS analysis of pin subsurface from Fig. 16. Bold signifies changes from the bulk microstructure.

Spectrum	C	O	Mg	Si	Mn	Fe	Cu	Zn
1	4.23	–	–	2.82	0.4	90.8	1.76	–
2	6.09	1.63	–	2.63	0.39	87.64	1.61	–
3	<b>73.97</b>	<b>7.38</b>	–	0.72	–	<b>17.62</b>	–	0.31
4	<b>73.6</b>	<b>5.82</b>	0.12	0.77	–	<b>19.41</b>	–	0.28

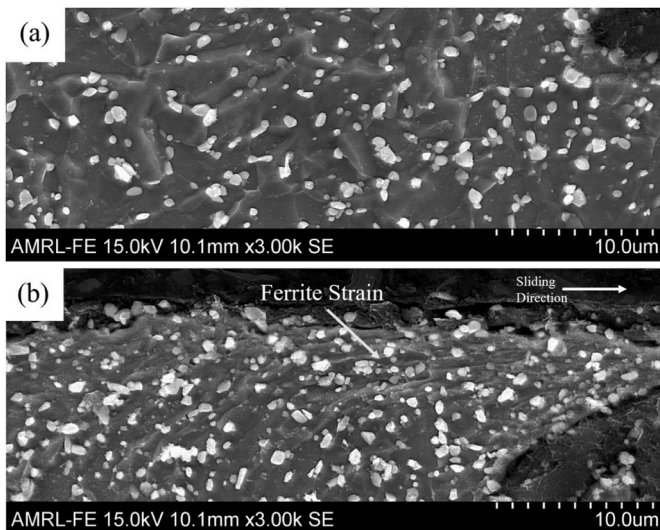


Fig. 18. (a) Bulk microstructure of 700C disc (b) subsurface deformation of 4 kg 700C. [x3000 – nital].

action. Apart from these local areas of damage, the majority of the worn area is similar in roughness and waviness to the milder scar, showing that mild oxidative wear is still the dominant mechanism at higher loads. This is also apparent in the roughness values,  $R_a$ , of the disc wear scars, which are mostly similar and in the same order apart from the most brittle disc at the highest load. A key difference between the findings of the present study and those of Ouyang et al. [5] is that no wear transition between mild and severe occurred for any samples or loads. The researchers [5] noted a transition to disproportionately higher volume losses when load increased beyond 90 N at 1.06 m/s, 80

N at 1.47 m/s, and 60 N at 1.88 m/s. However, as these variables are not consistent with the current study and through the use of different alloys, the exact points of transitions are likely to be different.

#### 4.4. The influence of hardness

The disc volume losses (Fig. 6) show that the 700C discs experienced the most wear, followed by 600C, 400C, and 500C. The acicular martensite outperforming the spheroidized structure is in agreement with the volume loss results obtained by Ouyang et al. [5], who found that the 4Cr13 stainless steel tempered at 550 °C lost more material than those tempered at 350 °C and 200 °C for all experimental conditions. In the present study, of the two acicular martensitic discs, the harder 400C was outperformed by 500C. This is due to excessive brittleness causing the 400C discs to have more local areas of mechanical damage. SEM inspection shows that the 400C discs display some areas of severe brittle ploughing/scoring while the 500C discs only show partially spalled oxide coverage (Figs. 8 and 11). The combination of these areas of mechanical damage and areas of mild oxidation, on the same 400C discs, are responsible for the high values of standard deviations in their roughness,  $R_a$ , values. The brittleness of the 400C discs is due to them having a combination of BCT crystal structure and acicular morphology, the combination of which is unique to the 400C discs. In contrast, the complete transformation to BCC ferrite allows the 500C acicular martensitic discs to deform more plastically, avoiding the brittle fracture mechanisms, and therefore only experience oxidative wear. The higher losses of the 700C discs are due to the inability of the microstructure to effectively support a protective oxide layer at the highest loads. Should the substrate deform and distort in a significant way, the oxide glaze layer destructs and the beneficial oxidation – scrape – re-oxidation [30] feedback loop does not arise. This is also accredited by Wei et al. [6] for why their H13 steel pins tempered at 700 °C experienced the highest volume losses.

Disc wear scar surface roughness trends, values, and standard deviations (Fig. 10) are indicative of their corresponding wear mechanisms. At 2 kg applied load, the roughness values are similar and display small standard deviations, as per the volume loss results (Figs. 6 and 7). At this load, little distinction exists because the majority of damage is only mild oxidative wear for all combinations. Oxidative wear is governed by surface conditions and testing parameters more so than microstructural condition, so at 2 kg, the various microstructural conditions have minor effects on wear mechanisms and therefore also the roughness.

Despite this, at 2 kg and 4 kg it can be observed that roughness increases with tempering temperature in accordance with the hardness measurements (Fig. 5) and volume loss results (Figs. 6 and 7). The higher tempering temperature produces spheroidized carbides in an equiaxed ferritic matrix (Fig. 3(c) and (d)), which increases the propensity for mild scoring and mild ploughing to occur, resulting in a rougher wear scar. The harder, acicular, microstructure of the 400C and 500C discs can resist such damage at 2 kg and 4 kg and thus produce smoother wear scars.

Additionally, as load increases to 4 kg, the 700C and 600C wear scars increase in roughness while 500C and 400C slightly decrease/remains at similar values. The increase for 600C and 700C is attributed to more plastic deformation causing perturbations on the wear scar surface. The minor decrease in roughness for 400C and 500C at 4 kg applied load is postulated to be caused by the similarity in wear mechanisms for these discs at 2 kg and 4 kg. As 400C and 500C both have acicular microstructures, they are resistant to plastic deformation and instead exhibit oxidative wear at both 2 kg and 4 kg, resulting in similar roughness values.

At 6 kg applied load, 700C, 600C, and 500C wear scars experience a reduction in roughness compared to 4 kg. Conversely, 400C increases in roughness and displays a large standard deviation. This increase is due to the inability of BCT martensite to plastically deform and therefore

experiences brittle fracture (Fig. 8(b)) which increases the measured roughness. These instances of brittle damage also corrupt the measurement of roughness, resulting in the large standard deviation seen for 400C at 6 kg. This is accomplished through the mixture of smooth intact surface morphology and brittle damage areas, the summation of which corrupts the measurement of Ra and gives a large scatter. The decrease in roughness for the other combinations is postulated to be due to increased plastic deformation resulting in more smearing than ploughing or scoring, which could smoothen out areas of graphite flake cavity spallation.

#### 4.5. Damage mechanisms

The annealed pin volume losses (Fig. 7) display similar values at 2 kg but diverge at 4 kg and 6 kg due to amplification of their different wear responses from the increased load. Although both disc and pin experienced low volume losses, the values of the pin are approximately double that of the discs, due to microstructural considerations (coarse pearlite/ferrite versus tempered martensite) and the effect of the tribosystem (such as the worn area of the disc being allowed to cool between cycles whereas the pin is unable to due to experiencing constant contact).

All samples exhibit spallation as a common damage mechanism due to the presence of graphite flakes. SEM inspection showed exposed graphite flake cavities on the surfaces of all sliding samples (Figs. 8, 12–14), indicating that flake cavity spallation is a damage mechanism that occurs for all loads and microstructural conditions. Exposed cavities frequently contain partial or full graphite flakes. Detached flakes can either be ejected onto, or sheared out along the sample surface, entering into the tribosystem. Evidence of graphite ejection in the form of 3D chips can be seen in the SEM inspection of the worn surfaces (Fig. 14(a)), while some evidence of beneficial shearing can be seen in the microstructural inspection of the subsurface (Fig. 18(b)).

Beneficial graphite solid lubrication smearing was not observed during SEM inspection of the worn surfaces. This could be due to a number of reasons, such as it being removed during the post-test treatment, mixed in with or indistinguishable from the surface oxides, thin-film coverage rendering it invisible, or it simply being a rare occurrence. The authors postulate that the latter is most likely, and that this rarity may be a result of the test conditions used, such as the relatively high sliding speed of 0.5 m/s for all tests. It is suspected that slower speeds would be more conducive to producing a beneficial graphite film due to the lower likelihood of graphite being expelled from the wear scar outward away from the samples, in addition to less destructive energy inputted to the contact faces which would allow for the flakes to beneficially smear. As previously mentioned, in-tact 3D chips of graphite were observed in several instances (Fig. 14(a)) on the worn surface of some samples, indicating that the expulsion of chips is more common than the smearing phenomena. Despite this, should graphite lubrication smearing occur, it is more likely to be arise for the 600C and 700C discs than the 400C and 500C discs, as it is known to occur more readily for alloys with softer matrices [31–33].

#### 4.6. Subsurface deformation

Subsurface microstructural deformation is important to analyse because it influences the subsequent wear occurring at the surface. Such subsurface microstructural deformation is visible in the annealed pins and spheroidized carbide discs (Figs. 16–18) but not in the acicular martensitic discs. Such deformation occurs due to a combination of load and speed inputting energy to the contact faces. This energy is dissipated through a number of ways such as heat, volume loss, transformation, and chemical reactions (oxidation), as discussed by Kato [34]. An additional energy output is through the deformation of the material under the wear surface. The volume loss results and SEM inspection of the worn pin end faces show that the pin experienced more damage than the discs. This repeated wearing of the pin surface results in subsurface

shear stresses which alters the directionality of lamellae. Subsurface deformation is highly localised due to grain orientation, where significant deformation can be seen in certain grains directly adjacent to others that show no signs of directionality.

The refinement and convergence process of cementite lamellae is a continuation of directional deformation. As lamellae are deformed in the direction parallel to the surface, the interlamellar spacing, and lamellae width, decreases. Successive refinement and convergence with surface oxides results in the conglomeration of cementite into a continuous carbide/oxide surface layer (Figs. 15(c) and 17). When analysed using EDS, carbon, and to a lesser extent, oxygen, show an increased concentration in the layer (Table 4). However due to the small size of the layer, the surrounding Bakelite was also within the x-ray scanning spot which may have influenced the elemental analysis. Subsurface deformation of this kind is beneficial in nature due to the refinement of lamellae resisting plastic deformation and crack propagation. Finer microstructures inhibit dislocation movement and are thus harder than coarser ones.

Cementite lamellae often fracture from deforming in the direction of sliding (Fig. 15(a) and ). This phenomenon is not uniformly constant, as many lamellae deform significantly without fracturing, whereas some fracture at relatively small angles of deformation. Plate thickness, 2D orientation, and curvature also do not correspond to lamella fracture. It is postulated that the primary influence is the 3D orientation of the cementite plate within the matrix, whereby excessive 3D curvature of the lamellae in a different direction to the sliding axis results in fracture. All sites of cementite plate fracture are accompanied by a dark area, postulated to be the void created from delamination of the cementite and ferrite matrix where the lamella originally resided. Such voids may be exacerbated by etching, where the nital may penetrate the delaminated area and result in localised crevice corrosion. Such fracture of lamellae and delamination of the lamellae-matrix interface is detrimental to further sliding wear resistance due to the stress concentrations surrounding such voids and their potential to serve as crack initiation sites.

Strained ferrite grains were the only visible subsurface feature seen in the carbide globule discs (600C and 700C) (Fig. 18). The carbides in these discs do not show directionality like the pearlitic pins as an innate consequence of their morphology. However, the ferrite grain strain is readily visible and more pronounced than in the annealed pins, due to the cementite lamellae in such pins being a barrier to matrix strain in most cases. Visible ferrite strain in this manner may also vary grain-to-grain due to local variations in the alloy chemistry. Vadiraj et al. [9] noted that wear resistance is a function of solid solution elements within the ferrite matrix. In the current study, local variations of such elements may be of significance, such as partially dissolved phosphide eutectic altering the ferrite wear resistance. Distorted ferrite grains are beneficial in sliding wear due to the increased hardness of the grain bestowing superior wear resistance and thus lowering material removal rates.

## 5. Conclusions

The present study investigated the pin-on-disc sliding wear response of G350 tempered martensitic grey cast iron discs against pearlitic pins of the same alloy. Four conditions of tempered martensite, and annealed pearlite/ferrite, were examined in the present study.

- A microstructural transition occurred when tempering between 500 °C and 600 °C. Tempering at 500 °C and below resulted in acicular martensitic microstructures, whereas tempering at 600 °C and above produced spheroidal carbide globules in equiaxed ferrite matrices.
- XRD showed that the 400C discs were partially BCT martensite while the other discs were BCC ferrite, indicating that the transformation to BCC ferrite is complete by 500 °C. The loss of the acicular martensitic

matrix in the 600C and 700C discs indicates that this evolution is complete by 600 °C.

- Hardness values decreased from 400HV for the 400C discs, to 315HV for 500C, to 230HV for 600C, to 215HV for 700C discs. The small decrease between 600C and 700C show that further tempering has minimal influence on indentation hardness. The annealed coarse pearlitic pins displayed a hardness of 215HV.
- Pin-on-disc sliding wear volume losses were low for all combinations. The 700C and 600C discs produced the highest volume losses due their spheroidal carbide microstructural morphology. Of the acicular martensitic discs, 400C showed higher volume losses than 500C due to excessive brittleness resulting in fracture of the matrix in some areas.
- Most combinations produced only mild oxidative wear. Residual grinding grooves were visible for most disc wear scars, indicating that the pin was unable to break-in to the disc surface. Many pins showed polished, reflective sections on the worn surface instead of metallic damage mechanisms. Due to the presence of graphite flakes, spallation was the most common mechanism to be seen for all samples.
- Microstructural subsurface deformation was visible in the annealed pins and spheroidized carbide discs. Cementite lamellae were deformed in the direction of sliding. Near the surface, lamellae were refined and converged into a mechanically mixed carbide/oxide layer. Lamellae would often fracture due to excessive deformation, however the occurrence of this is inconsistent and influenced by 3D factors. Strain distortion was visible in ferritic areas where the grain significantly deformed due to energy input from sliding.

#### Declaration of competing interest

The authors declare that they have no known competing financial interests or personal relationships that could have appeared to influence the work reported in this paper.

#### References

- [1] R. E. Smallman and A. H. W. Ngan, "Cast irons," in *Physical Metallurgy and Advanced Materials*, seventh ed., Elsevier, pp. 455–458.
- [2] ASM International, in: *Permanent Mold Casting*, vol. 15, Casting, 1998, p. 609.
- [3] H.T. Angus, Heat treatment of grey cast irons, in: *Cast Iron: Physical and Engineering Properties*, 1960, pp. 355–379.
- [4] ASM International, Heat treating cast iron, in: *Heat Treater's Guide: Practices and Procedures for Irons and Steels*, 1995, pp. 824–834.
- [5] J.H. Ouyang, Y.T. Pei, X.D. Li, T.C. Lei, Effect of tempering temperature on microstructure and sliding wear property of laser quenched 4Cr13 steel, *Wear* 177 (2) (1994) 203–208.
- [6] M.X. Wei, S.Q. Wang, L. Wang, X.H. Cui, K.M. Chen, Effect of tempering conditions on wear resistance in various wear mechanisms of H13 steel, *Tribol. Int.* 44 (7–8) (2011) 898–905.
- [7] C. Trevisiol, A. Jourani, S. Bouvier, Effect of hardness, microstructure, normal load and abrasive size on friction and on wear behaviour of 35NCD16 steel, *Wear* 388–389 (2017) 101–111. October 2016.
- [8] A.S.M.A. Haseeb, M.A. Islam, M.M. Ali Bepari, Tribological behaviour of quenched and tempered, and austempered ductile iron at the same hardness level, *Wear* 244 (1–2) (2000) 15–19.
- [9] A. Vadiraj, G. Balachandran, M. Kamaraj, E. Kazuya, Mechanical and wear behavior of quenched and tempered alloyed hypereutectic gray cast iron, *Mater. Des.* 32 (4) (2011) 2438–2443.
- [10] BSI Standards Online, BS EN ISO 945-1:2019, BSI Standards Publication: *Microstructure of cast irons*, 2019.
- [11] B. Bhushan, Wear of metals and alloys, in: *Introduction to Tribology*, second ed., Wiley, New York, 2013, p. 372.
- [12] I. Hutchings, P. Shipway, Sliding wear, in: *Tribology: Friction and Wear of Engineering Materials*, second ed., Butterworth - Heinemann, 2017, p. 293.
- [13] ASTM Standards, "ASTM G99 - 17: Standard Test Method for Wear Testing with a Pin-On-Disk Apparatus".
- [14] J.D. Verhoeven, Spheroidized microstructures, in: *Steel Metallurgy for the Non-metallurgist*, ASM International, 2007, pp. 35–37.
- [15] R.G. Woodward, A. Toumpis, A. Galloway, The influence of cementite spheroidizing duration on the microstructure and sliding wear response of grey cast iron against AISI 4330, *Wear* 488–489 (2022) 204155.
- [16] R.G. Woodward, et al., The influence of load on dry and tribocorrosive sliding of AISI 4330 and 15-5PH against cast iron the influence of load on dry and tribocorrosive sliding of AISI 4330 and, *Tribol. Trans.* 64 (5) (2021) 956–967.
- [17] G. Diao, Q. Yan, X. Shi, X. Zhang, Z. Wen, X. Jin, Improvement of wear resistance in ferrite-pearlite railway wheel steel via ferrite strengthening and cementite spheroidization, *Mater. Res. Express* 6 (10) (2019).
- [18] O.A. Zambrano, J.A. Gómez, J.J. Coronado, S.A. Rodríguez, The sliding wear behaviour of steels with the same hardness, *Wear* 418–419 (2019) 201–207. April 2018.
- [19] S. Bhattacharyya, Wear and friction in steel, aluminum and magnesium alloys I. Pearlitic and spheroidized steels, *Wear* 61 (1) (1980) 133–141.
- [20] F.H. Stott, The role of oxidation in the wear of alloys, *Tribol. Int.* 31 (1–3) (1998) 61–71.
- [21] F.H. Stott, G.C. Wood, The influence of oxides on the friction and wear of alloys, *Tribol. Int.* 11 (4) (1978) 211–218.
- [22] M.M. Stack, F.H. Stott, G.C. Wood, The effect of pre-oxidation of chromia and alumina forming alloys on erosion in laboratory simulated fluidized-bed conditions, *Corrosion Sci.* 33 (6) (1992) 965–983.
- [23] W. Hirst, J.K. Lancaster, Surface film formation and metallic wear, *J. Appl. Phys.* 27 (9) (1956) 1057–1065.
- [24] J.F. Archard, W. Hirst, The wear of metals under unlubricated conditions, *Proc. Roy. Soc. Lond. A.* 236 (1956).
- [25] T.F.J. Quinn, Review of oxidation wear. Part I: the origins of oxidation wear, *Tribol. Int.* 16 (5) (1983) 257–271.
- [26] T.F.J. Quinn, Role of oxidation in the mild wear of steel, *Br. J. Appl. Phys.* 13 (1) (1962) 33–37.
- [27] T.F.J. Quinn, The oxidation wear of low alloy steels, *Tribol. Int.* 35 (11) (2002) 691–715.
- [28] T.F.J. Quinn, W.O. Winer, The thermal aspects of oxidation wear, *Wear* 102 (1–2) (1985) 67–80.
- [29] T.F.J. Quinn, The effect of 'hot-spot' temperatures on the unlubricated wear of steel, *ASLE Trans* 10 (2) (1967) 158–168.
- [30] I. Hutchings, P. Shipway, Plasticity-dominated wear, in: *Tribology*, second ed., Elsevier Ltd., 2017, pp. 122–125.
- [31] J. Sugishita, S. Fujiyoshi, The effect of cast iron graphites on friction and wear performance I: graphite film formation on grey cast iron surfaces, *Wear* 66 (2) (1981) 209–221.
- [32] J. Sugishita, S. Fujiyoshi, The effect of cast iron graphites on friction and wear performance II: variables influencing graphite film formation, *Wear* 68 (1) (1981) 7–20.
- [33] J. Sugishita, S. Fujiyoshi, The effect of cast iron graphite on friction and wear performance III: the lubricating effect of graphite under rolling-sliding contacts, *Wear* 77 (2) (1982) 181–193.
- [34] K. Kato, Wear modes at asperity contacts in tribochemical wear, in: *Tribocorrosion of Passive Metals and Coatings*, 2011, p. 79.